WPMAT-PR(17) 17928

E. TEJADO et al.

Evolution of mechanical performance with temperature of W/Cu and W/CuCrZr composites for fusion heat sink applications

Preprint of Paper to be submitted for publication in
Materials Science and Engineering A

This work has been carried out within the framework of the EUROfusion Consortium and has received funding from the Euratom research and training programme 2014-2018 under grant agreement No 633053. The views and opinions expressed herein do not necessarily reflect those of the European Commission.

Evolution of mechanical performance with temperature of W/Cu and W/CuCrZr composites for fusion heat sink applications

E. Tejado[1], A. v. Müller[2,3], J-H. You[2], J.Y. Pastor[1]

[1] Departamento de Ciencia de Materiales-CIME,

Universidad Politécnica de Madrid, c/ Profesor Aranguren 3, E28040-Madrid, Spain

[2]Max-Planck-Institut für Plasmaphysik, 85748 Garching, Germany

[3]Technische Universität Munchen, 85748 Garching, Germany

CORRESPONDING AUTHOR:
Elena Tejado
Departamento de Ciencia de Materiales-CIME, Universidad Politécnica de Madrid, c/ Profesor Aranguren 3, E28040-*Madrid, Spain.*

Telephone: +34 91 336 52 43

Email: elena.tejado@upm.es

Abstract

Power exhaust and material lifetime have been identified as a key challenge for next generation fusion devices. For this purpose, water-cooled monoblock divertor, consisting of tungsten as plasma facing material and copper-based composites as the heat sink, have been proposed as the baseline materials. However, the large mismatch in the coefficient of thermal expansion and elastic modulus between these metals make it necessary the development of new interlayer composites.

In this context, the goal of this study is the mechanical and microstructural characterization of two composites materials, W-30 wt.%Cu and W-30 wt.%CuCrZr, produced by means of liquid Cu/CuCrZr infiltration in open porous W preforms. To achieve it, materials were analysed under high vacuum atmosphere (up to 10^{-6} mbar) between 25 and 800 ºC. From the mechanical characterization, dogbone-shape tensile tests and three-point bending fracture tests have been conducted. The impact of microstructure on the failure mechanism is also elucidated. A detailed study of the fractographic microstructure has been performed, aiming at providing physical interpretation of the tensile deformation and rupture behaviour.

Additionally, high temperature X-ray diffraction has been performed to check the stability and initial composition of the composites. From the XRD patterns, it was possible to assess that material system W-Cu/CuCrZr does not show any interfacial reaction or chemical degradation at operation temperatures, furthermore, the optimization of the manufacturing processes in an industrial environment has been assessed.

Keywords: Tungsten; copper; CuCrZr; Heat sink; Thermo-mechanical properties; MMC.

1. Introduction

The main plasma facing material (PFM) foreseen for next generation fusion devices are tungsten (W) and tungsten based alloys, since it combines high melting point, low sputtering rate, low vapour pressure and low retention of tritium. At the same time, copper (Cu) and its alloys, especially CuCrZr [1], have been widely studied for heat sink applications due to their high conductivity and high mechanical performance [2] [3]. Therefore, many design concepts for next fusion devices deals with W based materials joined to a Cu or CuCrZr heat sink. However, the lifetime of the joints is compromised by the high thermal stresses at the interface due to the mismatch in the coefficient of thermal expansion (CTE) and elastic modulus between both elements [4]. Additionally, the immiscible nature of W-Cu binary system, unblended even in liquid phase, make the joining a critical issue [5].

To overcome this problem, an interlayer material is needed. For this purpose, a metal matrix composite (MMC) between W and Cu could indeed tailor the CTE by controlling the composition and, hence, reducing the thermal mismatch. The interest of these MMC composites is twofold: the W matrix provides the necessary strength of the composite at high temperatures, while Cu and its alloys provide the required high thermal conductivity towards efficient heat removal in the cooling system.

Currently, powder metallurgy infiltration sintering method is commonly used in the preparation of Cu–W composites [6][7]. In this production route, a W skeleton with

proper relative density is compacted and sintered, and then, molten Cu is infiltrated into the porous of the structure. An extra sintering treatment is needed to obtain higher densifications [8]. The rigid skeleton structure of W determines the change in CTE, and the network structure of Cu benefits to the increase of thermal conductivity.

In this work, two MMC with compositions of W-30 wt.%Cu and W-30 wt.%CuCrZr have been produced by melt infiltration. Their thermophysical and mechanical properties were measured to assess their feasibility as a component of next generation fusion reactors.

2. Materials

The two MMC materials characterized in the present investigation were manufactured by infiltration of molten Cu and CuCrZr, respectively, in a W skeleton.

As first steep, an open porous W structure was produced by powder metallurgical route via uniaxial cold pressing. Later, consolidation at 1150 ºC for 2 h took place under hydrogen atmosphere. The porosity of the skeleton preform corresponds to a 70 wt. % W (52% pore volume fraction).

The infiltration of Cu and CuCrZr in the preform was performed at the previous conditions of pressure and temperature. Density measurements, by Archimedes method, revealed a residual porosity below than 5% for both materials. Further details on the production route and prior characterization can be found in [9]

Both, microstructure and fractography, were characterized by high resolution scanning electron microscopy (FEG-SEM), using a ZEISS AURIGA microscope (Carl Zeiss, Oberkochen, Germany) and Energy Dispersive X-ray spectroscopy (EDX).

Additionally, the microstructure was also investigated by High Temperature X-Ray Diffraction (HTXRD) with a PANalytical X'Pert PRO MPD diffractometer with a $Cu_{K\alpha}$ (λ=0.15405 nm) radiation source. Data were taken for the 2θ range of 20 to 90 degrees with steps of 0.001 degrees. Indexing process of powder diffraction pattern was done, and Miller Indices (h k l) to each peak were assigned in first step. In order to study the evolution of the composites with thermal exposure, the diffractograms were measured at different temperatures from 25 ºC to 800 ºC with 15 ºC/min ramp and 10 min dwell time, until stable conditions were achieved. All the measurements were acquired under vacuum conditions at $<10^{-5}$ mbar pressure.

The microstructure of the resulting materials after metallographic preparation can be observed in Fig. 1. In order to reveal the true metallographic microstructure, i.e. grain boundaries and higher contrast between the constituents, samples were previously etched with Murakami's reagent (100 ml water, 10 g NaOH and 10 g $K_3Fe(CN)_6$) and with a specific Cu etchant (60 ml Ethanol, 15 ml HCl and 5 g $FeCl_3$) for 10 s and 5 s, respectively.

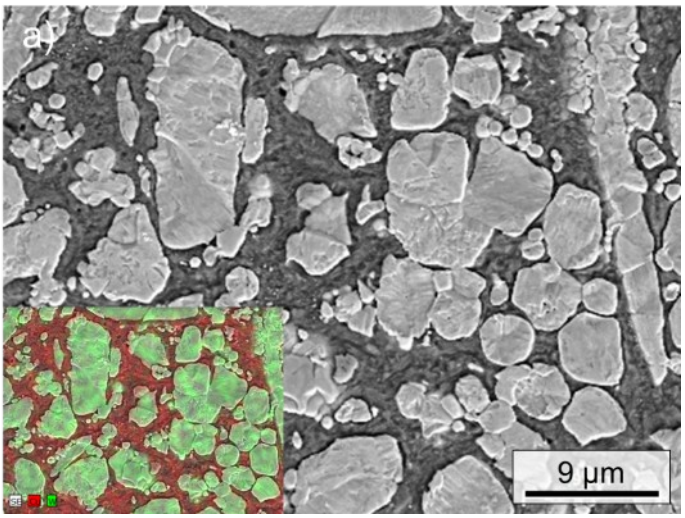

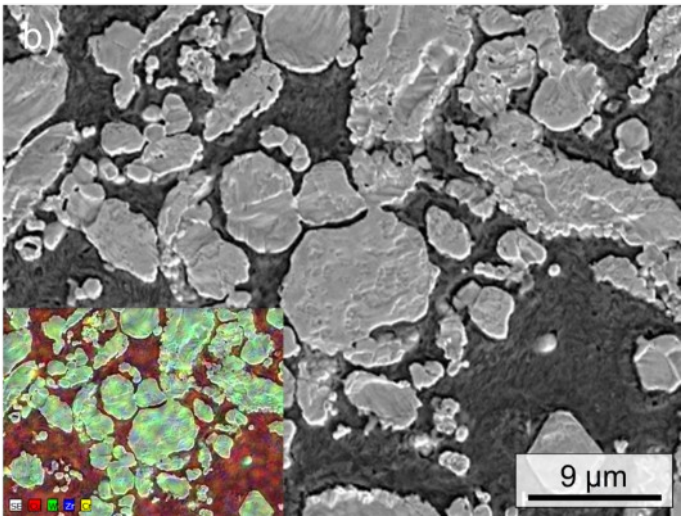

Fig. 1. SEM images and EDX map of a) W-30Cu and b) W-30CuCrZr composites after metallographic preparation and etching.

From the above images, it can be observed that the average grain size of W varies from several microns to dozens, while Cu forms an interconnected network structure around W particles. The interface between the W and Cu appears tight, without any interspace or porosity which is consistent with the high relative density (96%) measured.

Diffraction spectra of the samples were measured to conditions corresponding to testing temperatures, from 25 ºC to 800 ºC and the typical XRD patterns for the composites are shown in Fig. 2.

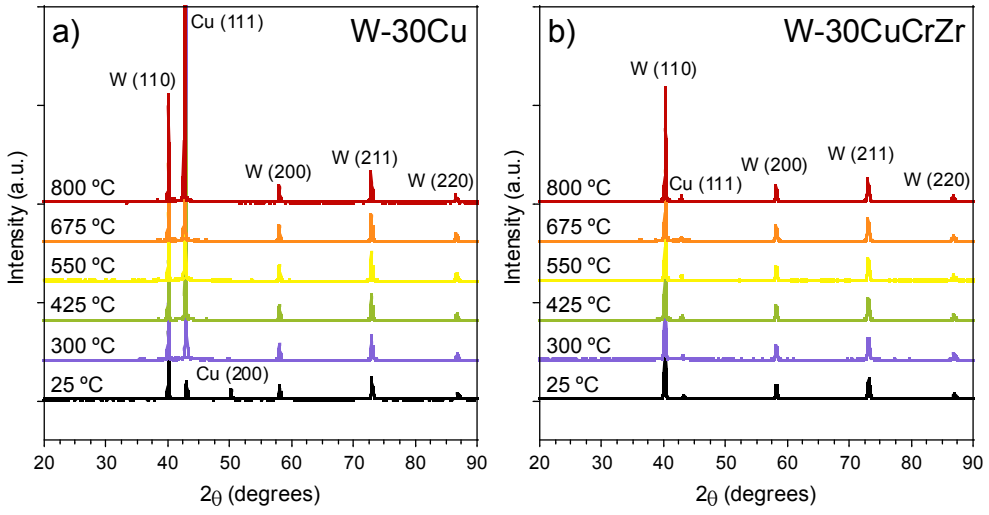

Fig. 2. XRD diffraction patterns of a) W-30Cu and b) W-30CuCrZr from 25 ºC to 800 ºC.

For W-30Cu, it is found that only metallic W (JCPDS: 4-0806) and Cu (JCPDS: 04-0836) diffraction peaks can be identified in spite of the variation of temperature. The absence of oxides indicates the success of conducting the manufacturing under preferable vacuum conditions. While the intensity and width of W reflections remain constant for all the temperature range, the peak intensity of the Cu(111) reflection at 43.29º strongly depended on the testing temperature, and raised by nearly three times from 9000 to 25000 counts per second (cps) for 25 and 800 ºC, respectively. This indicated a higher crystalline quality and/or orientation alignment for Cu at higher temperatures [10]. However, the average crystallite size, calculated using Scherrer formula from the linewidth of their respective XRD peaks, did not reveal grain growth for any of the components. These results are in accordance with the reported recrystallization temperature of bulk W between 900 ºC to 1400 ºC [11].

In the same way, the XRD pattern of W-30CuCrZr exhibited diffraction peaks at diffraction angles matching only with those of metallic W and Cu, with no evidence of precipitate phases. These results suggest that the precipitate phases are too tiny or sparse. It is noted that, in contrast to W-30Cu, the Cu(111) diffraction peak in W-30CuCrZr is weaker at all temperatures, which may suggests the solution of Cr or Zr in the Cu matrix, resulting in Cu lattice shrinkage as observed by [12] for CuCrZr alloys.

Thus, from the HTXRD it can be assess that no additional phases, i.e. interfacial reaction between W and Cu or CuCrZr, are induced by thermal exposure. Furthermore, the optimization of the manufacturing processes in an industrial environment has been assessed.

3. Experimental methods

Mechanical characterization was carried out in an INSTRON 8851 universal testing machine with a coupled environmental chamber, and at constant crosshead speed of 100 μm/min. All tests were conducted at room temperature (RT), 425, 550, 675 and 800 ºC using inductive heating at a heating rate of 10 ºC/min with 15 min dwell time and under very high vacuum atmosphere (10^{-6} mBar).

On the one hand, flexural strength and fracture toughness (K_{IC}) were tested in three-point bending (TPB) configuration on 2.8 mm×2.8 mm×25.0 mm barss. K_{IC} was determined by introducing a femto-laser notch in the bottom of the bars (Single-Edge-Laser-Notched-Bean, SELNB [13]). The stress intensity factor for mode I stress was then computed from the critical load (P_Q) and the beam section using the equation proposed by Guinea *et al.* [14]. The ASTM 5% secant method [15], i.e. a secant line with a slope equal to 95% of the initial elastic loading slope of the tangent line, was used to determine P_Q with the objective of defining the K_{IC} at the 2 % or less crack extension.

On the other hand, tensile tests were performed on dogbone shape samples where the size of the narrow portion of it was 2.0 mm×2.5 mm ×17.0 mm. The non-contact optical full field Digital Image Correlation (DIC) method was used to obtain the strain field during loading. DIC uses image registration algorithms to track the relative displacements of material points between a reference (typically, an undeformed zone) image and a current (typically, the deformed) image [16]. In this study, an open source 2D DIC MATLAB program called Ncorr [17] was used for the measurements and the further processing of the recorded displacement field. To measure the strain with the tensile tests, 2D deformation setup is required. Hence constant volume is assumed, only

one camera is needed. The experimental setup consisted of a tensile test machine, where the loading frame displacement was used for obtaining the engineering stress-strain curve. While the DIC system, with a high resolution camera (3840 px x 2748 px) coupled with an adequate light source, was set in front of the sample on a stable tripod to measure true strain over the loading area. Meantime, as tests were performed at elevated temperatures and under high vacuum, the DIC measurements were conducted through the window on the backside of the chamber, as validated previously by [18] and [19]. With this setup, it was possible to obtain resolutions higher than 10 μm/pixel.

To facilitate the DIC measurement, random speckle patterns were painted on the sample surface with a permanent marker. However, at temperatures above 600 °C only surface roughness, with its characteristic grayscale pattern, was used to calculate the displacement fields. Prior to the elevated temperature testing, a small mechanical load was apply to verify the symmetry of specimen and hence the uniaxial loading stage of it.

Elastic modulus, E, as a function of temperature were obtained from the load-deflection curves of the strength tests and then compared with the ones measured using Resonance Rrequency Analysis (RFA) at RT. A simple prediction with the rules of mixtures was also performed and Voigt, Resus and Hill modulus were used for defining the elastic modulus bounds. Materials data for the modulus of elasticity of W, Cu and CuCrZr were taken from[20], [21] and [22], respectively.

From the above results, it was also possible to estimate the uniaxial thermal expansion coefficient, α, of the composites. For this purpose, the empirical relation $E = 4.5\ \alpha^{-2.3}$ proposed by Arenz [23] was used. Where *E* is the elastic modulus measured from the bending tests. Here, energy well theory and thermodynamic analysis were employed to obtain the qualitative relationship.

4. Results

4.1. Fracture toughness

Fig. 3 shows the variation of fracture toughness as a function of temperature. For W-30Cu, the fracture toughness decreases rapidly from 17.5 MPa.m$^{1/2}$ at 25 ºC to 4 MPa.m$^{1/2}$ at 800 ºC. Additionally, the absolute fracture values are on average 25 % lower for W-30Cu than for W-30CuCrZr. Besides, this latter material exhibits a plateau region between 300 ºC and 550 ºC. Up to this temperature, the decrease is nearly constant. The local morphological configuration of the phases turns out to play an important role in triggering the fracture and subsequent failure.

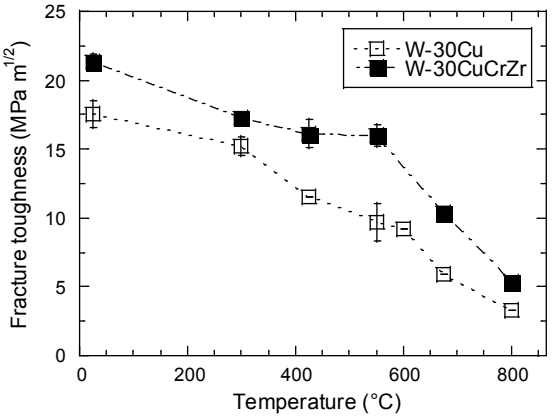

Fig. 3. Fracture toughness of the composites as a function of temperature and composition. Mean values and standard error.

4.2. Flexural strength

Fig. 4 shows the flexural strength of the WC-Cu composites at 0.2 % plastic strain, i.e. yield strength.

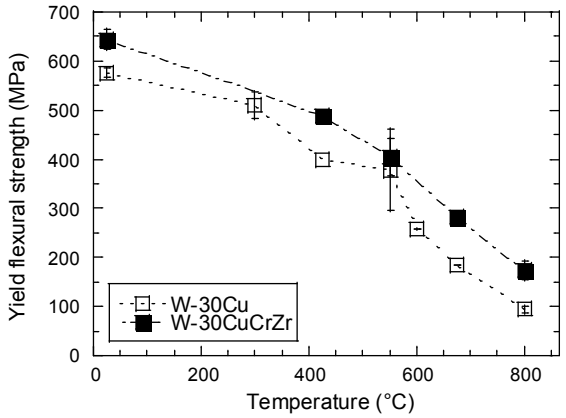

Fig. 4. Yield flexural strength of the composites as a function of composition and temperature. Mean values and standard error.

The flexural strength of the two composites exhibits the same trend: at 25 ºC both present values higher than 550 MPa but it decreases slowly up to 800 ºC. However, a slight recovery of the values is observed at 550 ºC for W-30Cu, but the error bars at this point are also higher. Furthermore, it can be seen that the material with a composition of W-30CuCrZr exhibits a yield flexural strength 50 % higher than W-30Cu in all the temperature range.

4.3. Tensile strength

Fig. 5 depicts the variation of yield and rupture strength of the composites after tensile testing. Tensile strength decreases as the testing temperature increases from 20 ºC to 800 ºC, for both materials. While values of yield and rupture strength follow the same trend in W-30CuCrZr, this behavior is not alike in W-30Cu composite. Hence, the softening and degradation of the Cu phase leads to relative low values of rupture strength.

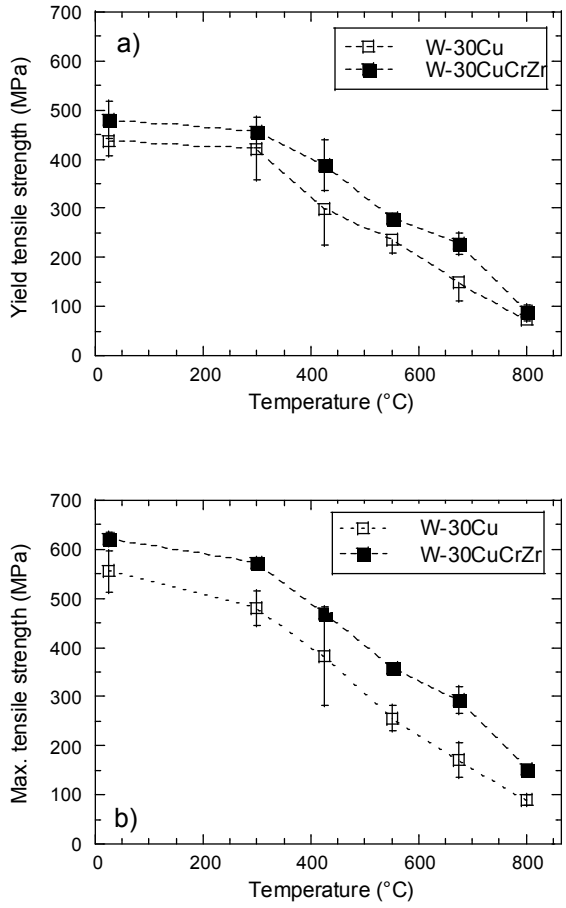

Fig. 5. a) Yield and b) maximum strength of the composites as a function of composition and temperature. Mean values and standard error.

The flow curves of the tests obtained at constant crosshead speed of 100 μm/min for W-30Cu and W-30CuCrZr are shown in Fig. 6 and Fig. 7, respectively. It is noticeable that the addition of Cu leads to a significant increase in maximum elongation at 425 ºC. At this temperature, both materials exhibit the highest values of rupture strain. However, the loss of strength of W-30CuCrZr composite is not so prominent at temperatures below 550 ºC. In addition, as observed for TPB tests, this material exhibits higher values of rupture stress and uniform elongation in tension. Up to 550 ºC both composites show relatively flat tensile stress-strain curves without any maximum, indicating and extensive plastic deformation and crack tip blunting without clear crack extension, i.e., the CuCrZr base alloy has relatively high

fracture toughness. These results are considerably better than the ones obtained by Zivelonghi and You [24] for a W-CuCrZr composite with 30 vol.% CuCrZr. They reported a maximum strength at 300 °C of around 350 MPa and close 200 MPa at 550 °C. As stated by them, the thermal stress caused by the thermal expansion mismatch between the constituents upon heating was the responsible of this behavior.

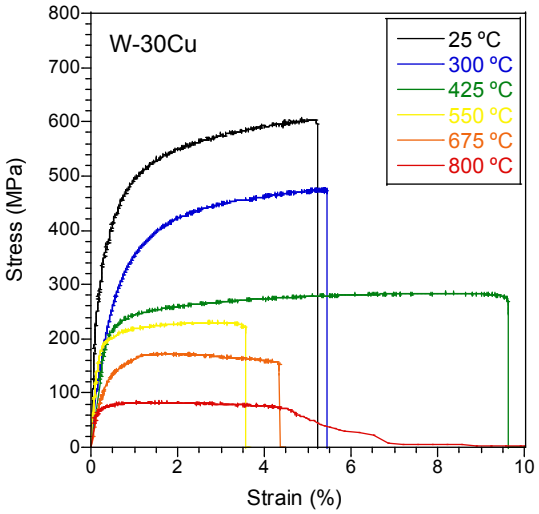

Fig. 6. True stress-strain curves for W-30Cu composite at different temperatures

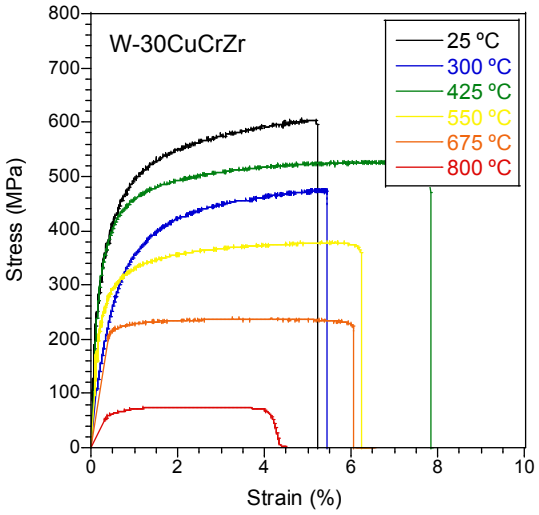

Fig. 7. True stress-strain curves for W-30CuCrZr composite at different temperatures

4.4. Elastic Modulus

Fig. 8 shows the variation of the elastic modulus as a function of temperature by measuring the slope of the strength curves. The elastic modulus decreases slowly from 175 GPa and 150 GPa, for W-30Cu and W-30CuCrZr respectively, to 110 GPa at 800 ºC, but the slope of W-30CuCrZr seems to be more moderate since its value at 25 ºC is lower. Nevertheless, the absolute values of elastic modulus are slightly higher for W-30Cu below 800 ºC. As testing temperature increases, so does the relative contribution of the W skeleton on the elastic properties, hence its degradation starts at higher temperatures. At higher temperatures, the effect of Cu or CuCrZr is residual so they tend to the same values.

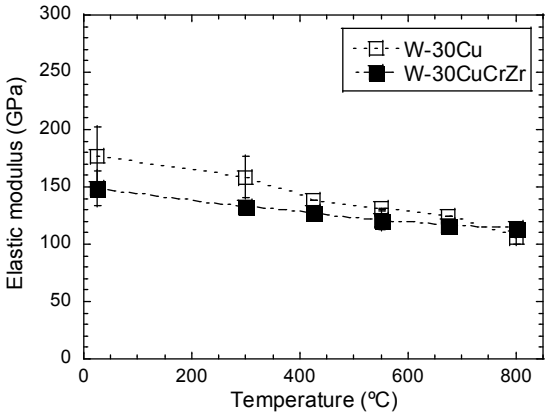

Fig. 8. Elastic modulus of W-30Cu and W-30CuCrZr as a function of composition and temperature. Mean values and standard error

Additionally, elastic modulus data are shown separately for each composition in Fig. 9. Results obtained from the Strength Tests (ST) have been compared with those obtained at 25 ºC with Resonant Frequency Analysis (RFA), and represented within the Voigt and Reuss boundaries. Hill average modulus is also shown. Furthermore, the residual porosity (4%) has been considered to avoid the overestimation of the predicted elastic constants.

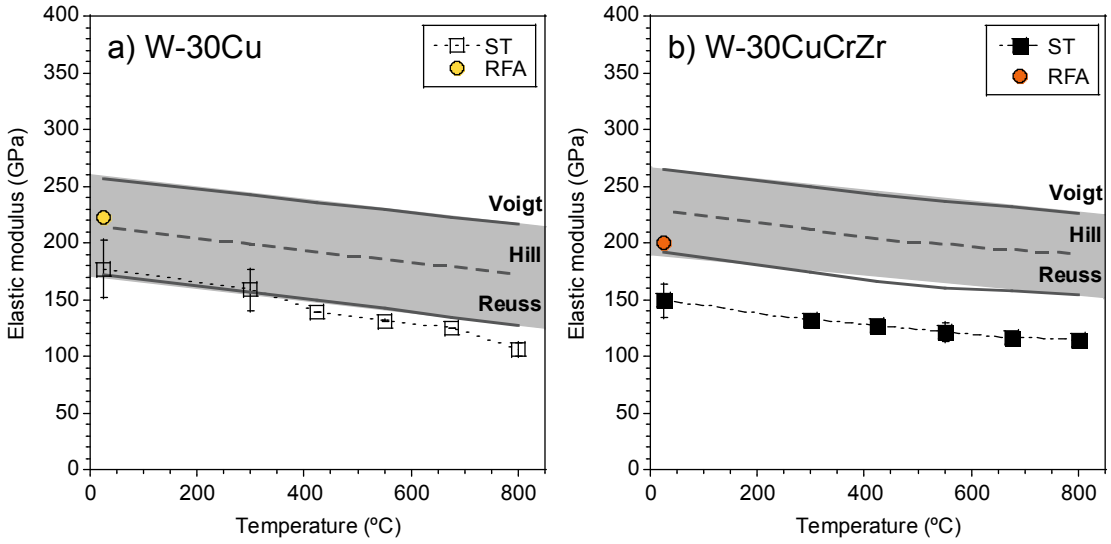

Fig. 9. Elastic modulus of a) W-30Cu and b) W-30CuCrZr as a function of temperature, mean and standard error. Values were measured from the strength tests (ST) curves and by Resonant Frequency Analysis (RFA). Upper and lower bounds were estimated with the Voigt and Reuss models, respectively, while Hill model is the average of them.

The values obtained from the strength curves of W-30Cu and Hill model match closely, as expected for a no-fibres composite [25]. However, the predicted bounds for W-30CuCrZr slightly overestimate the stiffness, although the observed trend is the same, i.e. the decreasing rate is lower up to 550 ºC. The difference between measured and predicted values may be attributed to the selected reference constants, hence literature values reported for CuCrZr alloys differs strongly from one another depending on the processing route and the thermal history of the alloy [26]. Metallurgical grade CuCrZr alloy have been selected as a reference in the present work. However, Papastergiou [27] reported the material data for its use in the JET hyper-vapotrons from studies of [28], both in hardened and aged condition. The value of the elastic modulus for the hardened material is indeed on average 30% higher than the data after aging (70 GPa to 100 GPa at RT). To obtain the hardened alloy, it was previously heated to 475 ºC for several hours and then quickly quenched so that no new crystal phases appear and its strength remains rather high. However, after operation at high temperatures, new crystal phases may appear in the grain boundaries. The aging of the material leads to its softening,

hence reducing the strength and elastic modulus while increasing the ultimate elongation. From the above studies, it can be asses that the CuCrZr phase in the composite W-30CuCrZr seems to be in an intermediate condition. Hence, hardened constants clearly overestimate the stiffness while aged condition slightly underestimates it.

On the other hand, elastic modulus values obtained from RFA are significantly higher than those measured by ST for both composites. Nevertheless, this mismatch has already been studied by others [29] [30] and it is caused mainly by the fact that the dynamic modulus was derived on the basis of the material being ideal on the macroscopic level, i.e. isotropic, homogeneous and elastic.

4.5. Thermal expansion coefficient

Fig. 10 depicts the variation of thermal expansion coefficient (CTE) of the W based composites with temperature. Literature values for CuCrZr and W from [31] and [32], respectively, are also represented for comparison. At each temperature, the thermal expansion coefficient monotonically increased with the temperature rise. However, the relative rate of change in the coefficient is around 1.6 $x10^{-3}$ $ºC^{-1}$, which is closer to the one exhibits by pure W (0.8 $x10^{-6}$ $ºC^{-1}$). In addition, there are not ample differences in the thermal expansion response of the two tested composites, hence, the skeleton structure of W determines the change in α, as its thermal expansion coefficient (4.6 10^{-6} $ºC^{-1}$) is five times lower than the one exhibits by Cu (17.0 10^{-6} $ºC^{-1}$) or CuCrZr (14.0 10^{-6} $ºC^{-1}$). These results are in good agreement with the ones obtained by Duan [33] for W–Cu composites produced by infiltration of Cu into W fiber preforms and by You [34] for infiltrated W-CuCrZr composites, though their research was conducted up to lower temperatures.

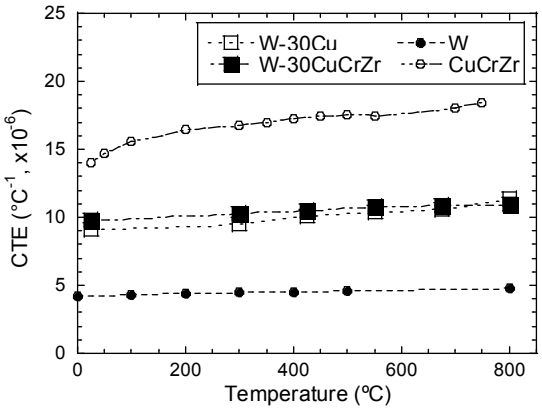

Fig. 10. Coefficient of linear thermal expansion of W-30Cu and W-30CuCrZr as a function of composition and temperature. Literature values for CuCrZr [31] and W [32] are also presented.

Many design concepts for next fusion devices deals with W or W alloys joined to a Cu or CuCrZr heat sink. However, the lifetime of the components is compromised by the high thermal stresses at the interface due to the mismatch in the CTE and elastic modulus between those materials [4]. The metal matrix composites presented in this article could effectively dissipate heat while tailoring CTE through the control of W skeleton porosity. This is of vital importance to enhance the performance, life cycle and reliability of the component.

5. Fractography

Fig. 11 shows the SEM images of the fracture surfaces after the strength tests. They clearly demonstrate the network of Cu that formed throughout the W skeleton. During the infiltration stage, molten Cu flows around W particles forming a homogeneous microstructure while filling the voids of the W skeleton, resulting in a high densification.

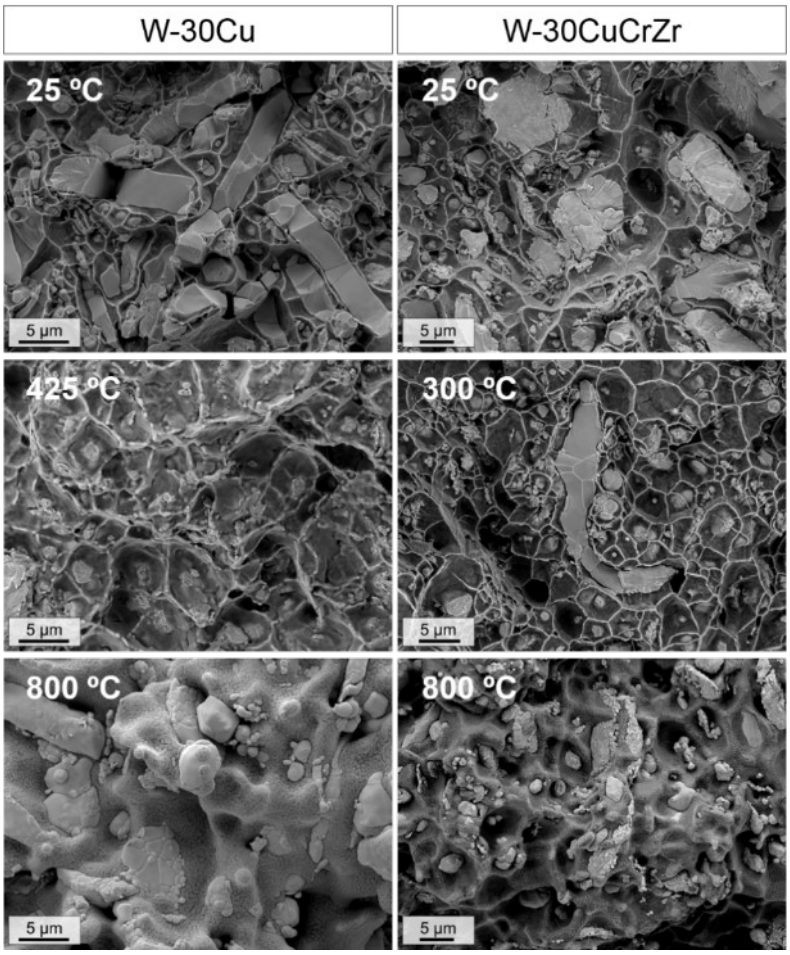

Fig. 11. Fracture surfaces for W-30Cu tested at 25 °C (top), 425 °C (middle) and 800 °C (bottom) in vacuum atmosphere. And for W-30CuCrZr tested at 25 °C (top), 300 °C (middle) and 800 °C (bottom) in vacuum atmosphere

As it can be appraised, both materials exhibit similar fracture surfaces. At 25 ºC, the predominant modes of fracture can be observed in left figures: transgranular fracture of W particles and plastic deformation of Cu matrix. This plastic behaviour can be illustrated by the number of fracture dimples: at room temperature, it is relatively low but it increases gradually with temperature up to 425 – 550 ºC where the composites reach the maximum elongation. The intrinsic brittleness of W matrix can also be observed with the transgranular cleavage patterns of W particles at low temperatures, with the existence of cracks that are propagated along the crystal planes during fracture process.

The degradation of the tensile performance up to 425 ºC can be explained through right figures that show the fractography of samples tested at 800 ºC. While W particles remain practically unaltered, Cu phase is clearly degraded because of the temperature increase.

High magnification images with EDX of W-30CuCrZr at three testing temperatures, 25 ºC, 425 ºC and 800 °C are shown in Fig. 12 and Fig. 13. From them, it can be noted that the interfacial bonding between W and CuCrZr is quite strong, as the ductile fracture surfaces of CuCrZr fully cover the surfaces of W particles. Small particles of Cr can be observed as well in Fig. 12(b), but it presence seems to be insignificant as no decomposition of CuCrZr alloy has been observed in other images.

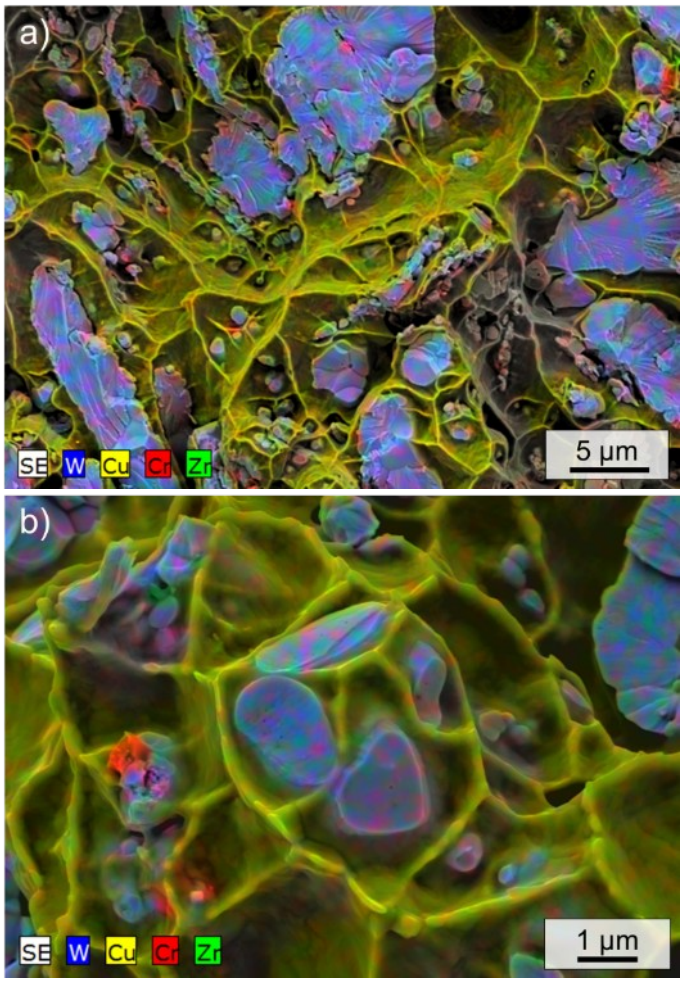

Fig. 12. EDX map of the fracture surfaces of W-30CuCrZr tested at a) 25 ºC and b) 425 ºC. For a better understanding of the surfaces, image of 425 ºC test is shown with higher magnification.

Upon viewing the following image, the thermal degradation of CuCrZr phase after testing at 800 °C is evident. The low values of tensile strength achieved by these materials at high temperature can be explained by the loss of resistance of the Cu phase and the subsequent loss of bonding to the W matrix. Furthermore, with the increase on temperature, the preferential fracture mode of W particles has shifted from a transgranular to intergranular one, since no brittle facets can be identified.

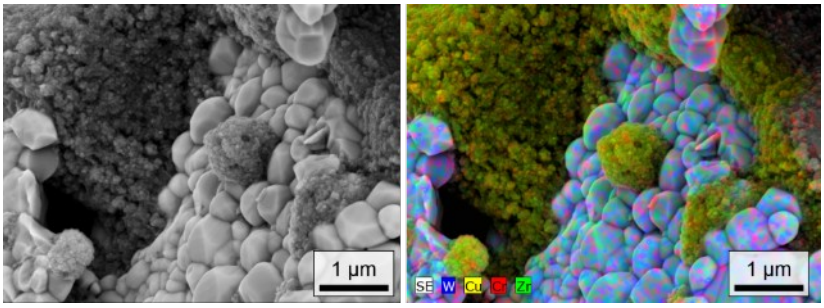

Fig. 13. Fracture surface of W-30CuCrZr tested at 800 °C. SE image and EDX map of composition

6. Conclusions

Thermal and mechanical properties of W-30Cu and W-30CuCrZr produced by means of liquid Cu and CuCrZr infiltration in open porous W preform have been studied. Testing campaign was performed up to 800 ºC under vacuum atmosphere (since over this temperature the performance of the materials is not relevant structurally), and values of fracture toughness, tensile and bending strength were obtained.

A remarkable temperature dependence can be asses from the measured mechanical properties. The yield strength of W-30CuCrZr is superior, as well as fracture toughness. On the other hand, elastic modulus and rupture strain are lower than the W-30Cu composite.

In addition, HTXRD has been accomplished to test the stability of the composites. From the XRD patterns, it was possible to assess that material system W-Cu/CuCrZr does not show any interfacial reaction or mutual solubility at operation temperatures. However, from the fracture surfaces, it was observed the the interfacial bonding of W and Cu/CuCrZr is quite strong even at high temperatures. These images revealed as well two kinds of fracture mechanisms: transgranular cleavage of W particles and ductility of both the Cu and CuCrZr phases, at low to middle temperatures.

The metal matrix composites presented in this article could effectively dissipate heat while tailoring CTE through the control of W skeleton porosity. Furthermore, the observed thermomechanical performance at relevant reactor temperatures could indeed overcome the thermal stresses produced during operation. This is of vital importance to enhance the performance, life cycle and reliability of the component.

7. Acknowledgements

This work has been carried out within the framework of the EUROfusion Consortium and has received funding from the Euratom research and training programme 2014-2018 under grant agreement No 633053. The views and opinions expressed herein do not necessarily reflect those of the European Commission.

The authors also acknowledge the support of the Ministerio de Economía y Competitividad of Spain (research project MAT2015-70780-C4-4-P) and the Comunidad de Madrid (research project S2013/MIT-2862-MULTIMATCHALLENGE) who have funded this research. Finally, we would also like to thank the Centro de

Asistencia a la Investigación (CAI) from the Excellence Moncloa-Campus (Madrid, Spain) for the thermo-diffraction measurements.

8. References

[1] H. Greuner, A. Zivelonghi, B. Böswirth, and J. H. You, "Results of high heat flux testing of W/CuCrZr multilayer composites with percolating microstructure for plasma-facing components," *Fusion Eng. Des.*, vol. 98–99, no. APRIL, pp. 1310–1313, 2015.

[2] ITER Joint Central Team, "The impact of materials selection on the design of the International Thermonuclear Experimental Reactor (ITER)," *J. Nucl. Mater.*, vol. 212–215, pp. 3–10, Sep. 1994.

[3] J. H. You *et al.*, "European DEMO divertor target: Operational requirements and material-design interface," *Nucl. Mater. Energy*, vol. 9, pp. 171–176, 2016.

[4] G. Pintsuk, S. E. Brünings, J. E. Döring, J. Linke, I. Smid, and L. Xue, "Development of W/Cu-functionally graded materials," *Fusion Eng. Des.*, vol. 66–68, pp. 237–240, 2003.

[5] D. Jiang *et al.*, "Femtosecond laser fabricated micro/nano interface structures toward enhanced bonding strength and heat transfer capability of W/Cu joining," *Mater. Des.*, vol. 114, pp. 185–193, 2016.

[6] A. Abu-Oqail, M. Ghanim, M. El-Sheikh, and A. El-Nikhaily, "Effects of processing parameters of tungsten-copper composites," *Int. J. Refract. Met. Hard*

Mater., vol. 35, pp. 207–212, 2012.

[7] P. W. Ho, Q. F. Li, and J. Y. H. Fuh, "Evaluation of W-Cu metal matrix composites produced by powder injection molding and liquid infiltration," *Mater. Sci. Eng. A*, vol. 485, no. 1–2, pp. 657–663, 2008.

[8] L. Xu *et al.*, "Influence of copper content on the property of Cu-W alloy prepared by microwave vacuum infiltration sintering," *J. Alloys Compd.*, vol. 592, pp. 202–206, 2014.

[9] A. v. Müller *et al.*, "Melt infiltrated tungsten–copper composites as advanced heat sink materials for plasma facing components of future nuclear fusion devices," *Fusion Eng. Des.*, pp. 1–5, 2017.

[10] L. Pranevičius, L. Pranevičius, and D. D. Milčius, *Tungsten Coatings for Fusion Applications*. VDU leidykla.

[11] T. Palacios, J. Reiser, J. Hoffmann, M. Rieth, A. Hoffmann, and J. Y. Pastor, "Microstructural and mechanical characterization of annealed tungsten (W) and potassium-doped tungsten foils," *Int. J. Refract. Met. Hard Mater.*, vol. 48, pp. 145–149, Jan. 2015.

[12] B. Zhang, Z. Zhang, and W. Li, "Mechanical properties, electrical conductivity and microstructure of CuCrZr alloys treated with thermal stretch process," *Trans. Nonferrous Met. Soc. China*, vol. 25, no. 7, pp. 2285–2292, Jul. 20115.

[13] T. Palacios and J. Y. Pastor, "Influence of the notch root radius on the fracture toughness of brittle metals: Nanostructure tungsten alloy, a case study," *Int. J. Refract. Met. Hard Mater.*, vol. 52, pp. 44–49, Sep. 2015.

[14] J. Y. Pastor, G. V. Guinea, J. Planas, and M. Elices, “NUEVA EXPRESIÓN DEL FACTOR DE INTENSIDAD DE TENSIONES PARA LA PROBETA DE FLEXIÓN EN TRES PUNTOS,” *An. Mecánica la Fract.*, vol. 12, no. 1995, pp. 296–301, 1995.

[15] ASTM Standard E1820-11, “Standard Test Method for Measurement of Fracture Toughness.” ASTM International, 2009.

[16] W. H. Peters and W. F. Ranson, “Digital imaging techniques in experimental stress analysis,” *Opt. Eng.*, vol. 21, pp. 427–431, 1982.

[17] J. Blaber, B. Adair, and A. Antoniou, “Ncorr: Open-Source 2D Digital Image Correlation Matlab Software,” *Exp. Mech.*, vol. 55, no. 6, pp. 1105–1122, 2015.

[18] S. T. Taher, O. T. Thomsen, and J. M. Dulieu-Barton, “Bidirectional Thermo-Mechanical Properties of Foam Core Materials Using DIC,” Springer, New York, NY, 2011, pp. 67–74.

[19] S. Zhang, J. M. Dulieu-Barton, R. K. Fruehmann, and O. T. Thomsen, “A Methodology for Obtaining Material Properties of Polymeric Foam at Elevated Temperatures,” *Exp. Mech.*, vol. 52, no. 1, pp. 3–15, Jan. 2012.

[20] J. M. Wheeler and J. Michler, “Invited Article: Indenter materials for high temperature nanoindentation,” *Rev. Sci. Instrum.*, vol. 84, no. 10, p. 101301, Oct. 2013.

[21] J. R. Davis and ASM International, *Copper and copper alloys*. ASM International, 2001.

[22] D. Qu, Z. Zhou, Y. Yum, and J. Aktaa, “Mechanical characterization and

modeling of brazed tungsten and Cu-Cr-Zr alloy using stress relief interlayers," *J. Nucl. Mater.*, vol. 455, no. 1–3, pp. 130–133, 2014.

[23] R. J. J. Arenz, "Relation of Elastic Modulus to Thermal Expansion Coefficient in Elastic and Viscoelastic Materials," *Sem*, no. 1, pp. 1–4, 2005.

[24] A. Zivelonghi and J. H. You, "Mechanism of plastic damage and fracture of a particulate tungsten-reinforced copper composite: A microstructure-based finite element study," *Comput. Mater. Sci.*, vol. 84, pp. 318–326, 2014.

[25] G. E. Totten and D. S. MacKenzie, *Handbook of aluminum*. Dekker, 2003.

[26] J. Y. Park, J. S. Lee, B. K. Choi, B. G. Hong, and Y. H. Jeong, "Effect of cooling rate on mechanical properties of aged ITER-grade CuCrZr," *Fusion Eng. Des.*, vol. 83, no. 10–12, pp. 1503–1507, 2008.

[27] S. Papastergiou, "Recent Advances in Reliability and Life Predictions of Critical JET Neutral Beam Components based on Realistic Material Data for DTE1 Operation and possible Upgraded Injector Scenarios," no. January, 1997.

[28] R. Tivey, "ITER Personal Communication," 1995.

[29] M. Radovic, E. Lara-Curzio, and L. Riester, "Comparison of different experimental techniques for determination of elastic properties of solids," *Mater. Sci. Eng. A*, vol. 368, no. 1–2, pp. 56–70, 2004.

[30] E. Tejado *et al.*, "The effects of tantalum addition on the microtexture and mechanical behaviour of tungsten for ITER applications," *J. Nucl. Mater.*, vol. 467, 2015.

[31] Y. Birol, “Thermal fatigue testing of CuCrZr alloy for high temperature tooling applications,” *J. Mater. Sci.*, vol. 45, no. 16, pp. 4501–4506, Aug. 2010.

[32] P. Hidnert and W. T. Sweeney, “Thermal Expansion of Tungsten,” *Sci. Pap. Bur. Stand.*, vol. 20, pp. 483–487, 1925.

[33] L. Duan, W. Lin, J. Wang, and G. Yang, “Thermal properties of W-Cu composites manufactured by copper infiltration into tungsten fiber matrix,” *Int. J. Refract. Met. Hard Mater.*, vol. 46, pp. 96–100, 2014.

[34] J. H. You, A. Brendel, S. Nawka, T. Schubert, and B. Kieback, “Thermal and mechanical properties of infiltrated W/CuCrZr composite materials for functionally graded heat sink application,” *J. Nucl. Mater.*, vol. 438, no. 1–3, pp. 1–6, 2013.